



**HAL**  
open science

# Qualitative analysis of a 3D multiphysics model for nonlinear ultrasonics and vibration induced heating at closed defects

Kevin Truyaert, Vladislav Aleshin, Koen van den Abeele

► **To cite this version:**

Kevin Truyaert, Vladislav Aleshin, Koen van den Abeele. Qualitative analysis of a 3D multiphysics model for nonlinear ultrasonics and vibration induced heating at closed defects. *Research in Nondestructive Evaluation*, 2022, 33 (1), pp.17-32. 10.1080/09349847.2022.2049408 . hal-03747601

**HAL Id: hal-03747601**


**<https://hal.science/hal-03747601v1>**

Submitted on 15 Nov 2022

**HAL** is a multi-disciplinary open access archive for the deposit and dissemination of scientific research documents, whether they are published or not. The documents may come from teaching and research institutions in France or abroad, or from public or private research centers.

L'archive ouverte pluridisciplinaire **HAL**, est destinée au dépôt et à la diffusion de documents scientifiques de niveau recherche, publiés ou non, émanant des établissements d'enseignement et de recherche français ou étrangers, des laboratoires publics ou privés.

# Qualitative analysis of a 3D multiphysics model for nonlinear ultrasonics and vibration induced heating at closed defects

Kevin Truyaert<sup>1,\*</sup> , Vladislav Aleshin<sup>2,3</sup> and Koen Van Den Abeele<sup>1</sup>

<sup>1</sup> KU Leuven campus Kulak, B-8500 Kortrijk, Belgium

<sup>2</sup> Univ. Lille, CNRS, Centrale Lille, ISEN, Univ. Valenciennes, UMR 8520-IEMN, LIA LICS/LEMAC, F-59000 Lille, France

<sup>3</sup> Tomsk State University, 634050 Tomsk, Russia

\* Correspondence: kevin.truyaert@kuleuven.be

**Abstract:** Upon exciting a material using elastic waves, the locally induced deformation at the interfaces of internally closed defects may cause nonlinear wave mechanics and dynamics in the form of clapping and friction. As a result, both phenomena instigate spectral broadening of the excitation spectrum as well as the production of heat, directly originating from the defect. To better understand and account for the physics behind the dissipation of energy by internally closed defects as a result of the wave-interface interaction, dedicated models can be developed. In this work, we propose a 3D finite element multiphysics model that is capable of simultaneously describing the generation of nonlinearities and heating at a defect's interface experiencing clapping and friction induced by elastic wave propagation. The model consists of three different modules. The first module describes the elastic wave propagation in a virgin/bulk material, whereas the second module captures the contact physics at the defect level. The third module is implemented to calculate the diffusion of thermal energy in the specimen. The contact physics module accounts for anharmonic and hysteretic effects, describing the nonlinear behavior of the defect's interfaces, which is echoed in both the ultrasound spectrum and in the vibration induced heating. A qualitative analysis of the computational model, integrating the three modules, is performed to validate the approach. Examples show that nonlinear spectral components are indeed observed as a result of the friction and the clapping experienced by the faces of the defect. At the same time, a localized temperature increase due to the induced friction is noted, and its response at the outer surface of the sample is examined. The qualitative validation approves that the model is ready to be tested further quantitatively, and to compare its predictions to experiments.

**Keywords:** Ultrasound; Modelling; Friction

**Citation:** Truyaert, K.; Aleshin, V.; Van Den Abeele, K. Qualitative analysis of a 3D multiphysics model for nonlinear ultrasonics and vibration induced heating at closed defects. *Journal Not Specified* **2021**, *1*, 0. <https://doi.org/>

Received:

Accepted:

Published:

**Copyright:** © 2021 by the authors. Submitted to *Journal Not Specified* for possible open access publication under the terms and conditions of the Creative Commons Attribution (CC BY) license (<https://creativecommons.org/licenses/by/4.0/>).

## 1. Introduction

Ultrasonic vibrothermography is an auspicious Non-Destructive Testing (NDT) technique for the detection of closed defects, either fully internal or surface breaking. The principle of ultrasonic vibrothermography is simple: through excitation by ultrasonic waves, frictional behavior at the defect's interfaces takes place. As a result, the vibrational energy of the elastic wave will locally be converted into thermal energy, generating heat around the defect, which subsequently dissipates through the medium by way of thermal diffusion. In practice, the distributed heat can be recorded by an infrared camera, possibly detecting the heat signature and its origin. Next to defect detection, defect characterization has become one of the major research interests in NDT, in particular to anticipate the severity of the defect. However, to obtain reliable and high quality defect classification by ultrasonic thermography, theoretical models capable of interpreting the obtained thermograms are necessary.

Contact models come in all shapes and sizes. Some models only take into account clapping (the normal behavior) [1], but more realistic models also include friction (the tangential behavior). The contact profile of the two bodies in contact also greatly influences the response of the applied loading procedure. Some studies assume the bodies in

39 contact to have flat faces [2] whereas other models introduce non-flat surface, allowing  
40 to account for roughness [3–7]. When a nontrivial topography at the contact area is  
41 assumed, a contact situation of partial slip needs to be introduced, next to the two trivial  
42 contact states of contact loss and sliding. In the partial slip state, both stick and slip areas  
43 can be simultaneously present at the contact interface, as a result of Coulomb’s frictional  
44 law. For the implementation into the model, the difficulty of meshing all asperities at the  
45 contact faces on a microscopic level is avoided by considering a multiscale approach in  
46 which mesoscopic cells are introduced in the mesh. Using this approach in a 1D (normal)  
47 loading, the complexity of the stress and displacement fields, along with the contact  
48 profile and possible roughness can be fitted into a single relationship between normal  
49 displacement and normal load.

50 The authors of this work, together with others, previously developed a 2D contact  
51 model. The description of the contact model follows the Method of Memory Diagrams  
52 (MMD) to update the contact loads in a semi-analytical manner, not needing to approach  
53 the state of the load through variational means [4,5]. Apart from updating the stress at  
54 the level of the contact, the 2D contact model is also capable of calculating the instan-  
55 taneously generated heat induced by friction at the contact interface [8,9]. Traditional  
56 implementations on the calculation of dissipated energy generally start from the as-  
57 sumption of cyclic contact behavior, hence a simple closed hysteretic loop, and calculate  
58 the area of the hysteric loop to find the dissipated energy per cycle [10,11]. However,  
59 despite the fact that the loading procedure may be monofrequent, internal reflections and  
60 nonlinear effects will result in complex contact behavior, creating complicated and/or  
61 non-closed, hysteretic areas, instead of a single closed loops. Apart from this, having  
62 non-static conditions, such as an evolving crack, fatigue of the material, a changing  
63 excitation amplitude or frequency as an influence of the bond between actuator and  
64 sample ... will also have an effect on the hysteresis area. Therefore, the instantaneous  
65 energy dissipation method has been extended to accommodate the MMD contact model  
66 as illustrated in previous work for realistic excitation procedures in 2D case studies [8].  
67 Also a passive excitation will result in a nonperiodic contact behaviour as well, making  
68 this method of calculating the dissipated energy also valuable for modelling structural  
69 health monitoring scenarios through passive excitations. The 2D simulation model  
70 clearly reveals the simultaneous presence of nonlinear elastic wave generation, i.e. the  
71 generation of higher harmonics of the excitation frequency at the defect location, along  
72 with the thermographic response at the defect and its radiation towards the boundaries.

73 In the present contribution, we develop and discuss a three dimensional model,  
74 based on the aforementioned two dimensional model. We perform a qualitative analysis  
75 by comparing the obtained numerical results to results described in the literature in  
76 order to validate the capability of the three dimensional model to simulate realistic  
77 situations.

## 78 2. Materials and Methods

79 As the current three dimensional model is based on the previous two dimensional  
80 model described by the authors of this work, the most important ingredients of the  
81 computational model will be briefly recapped [4,5,8]. The model consist of three different  
82 modules. The first module describes the elastic wave propagation in a virgin material.  
83 The second module captures the contact physics at the defect level. This module accounts  
84 for anharmonic and hysteretic effects, describing the nonlinear behavior of the defect’s  
85 interfaces, which is echoed in both the ultrasound spectrum and in the vibration induced  
86 heating. The third module is implemented to calculate the diffusion of thermal energy  
87 within the specimen. The full model is built in COMSOL Multiphysics<sup>®</sup> and uses its  
88 internal descriptions for the first and third module. The contact response is described  
89 through the Method of Memory Diagrams (MMD) in three dimensions and is linked to  
90 the computational model through a MATLAB<sup>®</sup> interface.

## 91 2.1. Contact description

92 By combining the above contact description with the two modules to solve the wave  
 93 equation in bulk materials and the heat transfer equation in solids, a consistent model  
 94 can be built to simulate the nonlinear elastic behavior and the vibrothermal response at  
 95 the defect's contact faces. These are reflected in the nonlinear spectral components in the  
 96 frequency spectrum and in the thermograms. The extension of the MMD description  
 97 in 3D can be retrieved in analogy with the two dimensional case. The MMD contact  
 98 model represents a semi-analytical method that allows to study the dynamic response of  
 99 a hysteretic tangential contact in the simultaneous presence of a normal contact loading,  
 100 respectively describing friction and clapping. The normal ( $\sigma$ ) and tangential ( $\vec{\tau}$ ) loads  
 101 are calculated in each point, given the normal indentation  $a$  and tangential displacement  
 102  $\vec{b}$  at that location. The method accounts for roughness at the internal boundaries of the  
 103 internal defect, assuming the asperities are convex and axisymmetric, following the  
 104 Mindlin description on contact mechanics [12] and the reduced elastic principle [13,14].  
 105 These assumptions allow to avoid an expensive computational procedure of updating  
 106 the stress profiles to the current position by introducing analytical functions that need  
 107 to be iteratively updated, as the contact progresses. As mentioned in the introduction,  
 108 roughness at the contact interfaces introduces a contact state called partial slip when  
 109 the tangential load is smaller than the product of the frictional coefficient ( $\mu$ ) and the  
 110 normal load, i.e. when the Coulomb condition for slipping is not yet met ( $|\tau| \leq \mu\sigma$ ).  
 111 These microscopic asperities, which are assumed to be convex and axisymmetric, are  
 112 locally unified in a general mesoscopic cell (which will be the size of the mesh element  
 113 in the simulations) and generalized into one single convex axisymmetric profile, which  
 114 exerts an equivalent load to the opposing face. These equivalent loads result in an  
 115 identical contact behaviour compared to the original family of asperities. Sub-figure (a)  
 116 of Figure 1 shows an axisymmetric contact in a state when no tangential displacement is  
 117 applied, after the center of the contact has been indented over a distance  $q$ . Sub-figure (b)  
 118 represents the status of the contact area obtained by increasing the normal indentation  
 119 to distance  $a$  at the center after which a non-zero tangential displacement is applied. As  
 120 the contact profile is convex, the outer regions will experience a smaller normal load  
 121 compared to the interior region. Subsequently, the Coulomb friction criterion will be met  
 122 in the outer regions ( $|\tau| = \mu\sigma$ ), as the tangential load is the same in the entire contact  
 123 region. As of this, regions with a radius between  $s$  and  $c$  will generate friction, whereas  
 124 the inner contact region (with a radius smaller than  $s$ ) will remain in place and does not  
 125 slide, as  $|\tau| \leq \mu\sigma$  in this region.

126 To implement the presence of stick, slip and partial slip into the contact model, the  
 127 normal and tangential loads acting in each point of a contact need to be determined. This  
 128 can be done by relating them to the displacements. The load-displacement relationship  
 129 which accounts for the normal dimension is based on both an empirically [15] and a  
 130 numerically [16] derived quadratic relationship:

$$\sigma = C \cdot a^2, \quad (1)$$

131 where  $C$  is a material dependent constant and is  $3.6 \cdot 10^{21} Pa \cdot m^{-2}$  for aluminium. The  
 132 tangential interaction occurs through the MMD, where the piece-wise memory vector  
 133 function  $\vec{D}(\alpha)$  plays the central role, containing the memory of the hysteretic contact.  
 134 This vector function is updated through the current tangential displacement vector  $\vec{b}$   
 135 and used to calculate the tangential load vector  $\vec{\tau}$ :

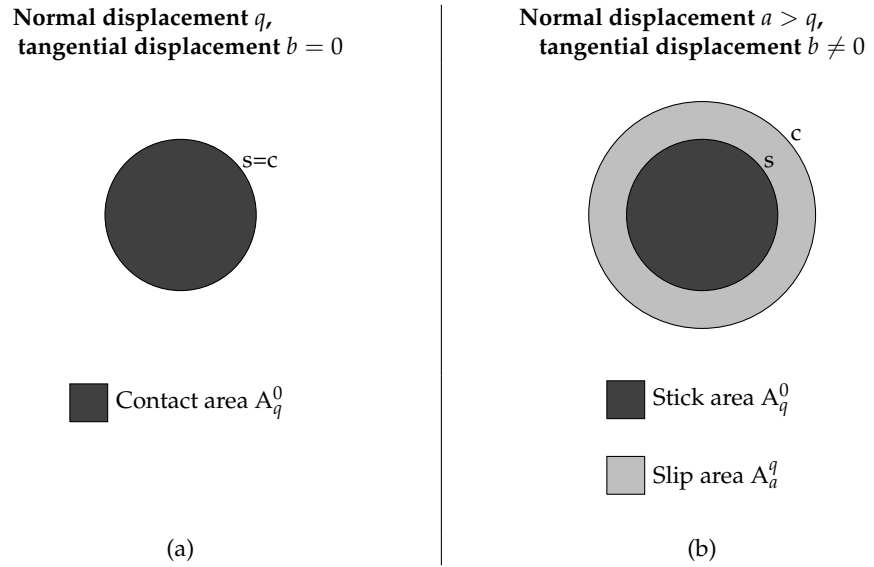


**Figure 1.** Representation of the 3D axisymmetric contact description, as a generalization of a set of arbitrary contacts, experiencing no tangential displacement (figure a) versus experiencing a tangential displacement (figure b). As a tangential loading is applied to the system, at some contact points, the Coulomb threshold will be met, introducing slip inside the regions with a radius between  $s$  and  $c$ , where  $c$  is the radius of the contact and  $s$  is the radius of the stick area. The more central parts of the contact, due to the convex assumption of the contact, will not experience slip, as the Coulomb threshold is not met.

$$\left\{ \begin{array}{l} b_x = \theta \mu \int_0^a D_x(\alpha) d\alpha \\ b_y = \theta \mu \int_0^a D_y(\alpha) d\alpha \\ \tau_x = \mu \int_0^a D_x(\alpha) \frac{d\sigma(\alpha)}{d\alpha} d\alpha \\ \tau_y = \mu \int_0^a D_y(\alpha) \frac{d\sigma(\alpha)}{d\alpha} d\alpha \end{array} \right. , \quad (2)$$

136 where  $\theta$  is a material parameter which depends on Poisson's ratio  $\nu$  [4]. The rules follow  
 137 the exact same steps as in the 2D case, as explained and illustrated in [4], except that  
 138 the orthogonal parts of the memory vector function  $\vec{D}(\alpha)$ , now comprise an area of  
 139 maximum  $\cos \gamma$ , respectively  $\sin \gamma$ , where  $\gamma$  is the angle of the tangential displacement,  
 140 as they represent orthogonal projections of  $\vec{\tau}$ . Note that we have assumed isotropy at  
 141 the moment for the material parameters  $\theta$  and  $\mu$ , however, an extension to anisotropic  
 142 media can be obtained by including the tensor notation of  $\theta$  and  $\nu$ .

143 The energy dissipation in 3D, which determines the amount of energy lost due to  
 144 friction, can be retrieved in a similar way as in the 2D case, as has been described in  
 145 Truyaert et al. [9]. This energy is calculated as the inner product of both the tangential  
 146 load ( $\vec{\tau}(\rho)$ ) and the tangential slip ( $\Delta\vec{\Sigma}(\rho)$ ), inside the slip region,

$$\Delta W = \int_s^c (\vec{\tau}(\rho) \cdot \Delta\vec{\Sigma}(\rho)) 2\pi\rho d\rho. \quad (3)$$

147 In this expression, the lower and upper boundaries of the integral,  $s$  and  $c$ , denote the  
 148 radii of the related circles describing the contact, as depicted in Figure 1. Equation 3 can  
 149 be conveniently rewritten in terms of the displacement vectors and normal load, which  
 150 are all inputs of the model, in order to obtain,

$$\Delta W = 2\mu \left[ \left\| \vec{\Delta b} \right\| - \theta\mu\Delta a \right] \cdot \left( \sigma(a) - \sigma(q) + \frac{d\sigma}{da} \Big|_{a=q} (q - a) \right), \quad (4)$$

151 where  $q$  corresponds to the normal indentation which would be needed to obtain the  
 152 non-slipping contact region, as in the right part of Figure 1, and  $\left\| \vec{\Delta b} \right\|$  is the Euclidean  
 153 norm of the tangential slip displacement vector.

## 154 2.2. Computational model

155 By combining the above described nonlinear and history dependent contact me-  
 156 chanics with the two modules to both solve the wave equation in bulk materials and the  
 157 heat transfer equation in solids, a consistent model can be built to simulate the nonlinear  
 158 dynamics of the defect's contact faces. These microscopic and mesoscopic features will be  
 159 reflected in the macroscopically observable nonlinear spectral components and thermal  
 160 properties. Simulations performed with the developed model need to be time-dependent  
 161 in order to correctly capture the generation of the nonlinear effects.

162 The time stepping procedure, of which a flowchart is present in Figure 2, is as  
 163 follows:

### 164 (a) Computation of displacements and temperature distribution

165 Starting from the local normal and tangential stresses ( $\sigma$  and  $\vec{\tau}$ ), the Structural  
 166 Mechanics module of COMSOL<sup>®</sup> calculates the displacements within the entire  
 167 domain at each time instance  $t$  of the procedure. The local normal and tangential  
 168 displacements ( $u_n$  and  $\vec{u}_t$ ) on the contact interface are stored as output of the  
 169 COMSOL<sup>®</sup> module, and used as an input for the displacement driven MMD  
 170 module which is implemented in MATLAB<sup>®</sup> in the next calculation step (see (b)).  
 171 Simultaneously, the heat diffusion problem in response to an internal boundary  
 172 heat source at the contacting surfaces is solved through the Heat Transfer module  
 173 of COMSOL<sup>®</sup>, updating the temperature distribution in the entire computational  
 174 region. In contrast to the contact module which is only addressed for the defect spe-  
 175 cific nodes, the PDE's for structural mechanics and thermal diffusion are constantly  
 176 updating all properties in the whole computational region.

### 177 (b) Computation of contact stresses and energy losses

178 During this intermediate step, the parameters at the contact interface are updated.  
 179 The displacement-driven MMD module for the nonlinear and history dependent  
 180 contact dynamics, implemented in MATLAB<sup>®</sup>, calculates the new stress parameters  
 181 at the integration points on the contact interface. Simultaneously, the friction-  
 182 induced energy loss is calculated for each of these points. The calculated stress  
 183 values and energy losses are then returned to COMSOL<sup>®</sup> in order to update  
 184 the mechanical (i.e. internal thin elastic layer) and thermal (i.e. internal heat  
 185 source) boundary conditions at the contact interface in respectively the Structural  
 186 Mechanics and Heat Transfer modules. In this step, only the boundary conditions  
 187 at the defect interface are updated.

### 188 (c) Repeated calculations

189 Steps (a) and (b) are repeated for the next time instance  $t + \Delta t$ , continuously  
 190 updating the entire computational region first and then the boundary conditions  
 191 on the crack. This goes on until the desired calculation time is reached ( $t = t_{\text{end}}$ ).

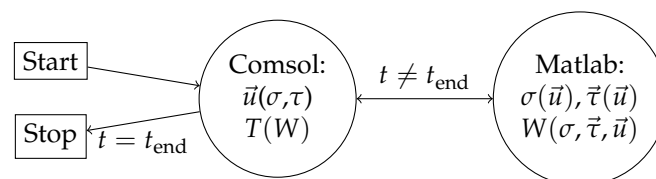


**Figure 2.** Small flowchart of the computational procedure where the locations of the updates of parameters related to the contact description are highlighted.



**Figure 3.** Geometry of the more complex cut.

192 Both the structural mechanics and thermal module are solved using an appropriate  
 193 mesh, with its corresponding discretizations and shape functions to the order of the  
 194 chosen mesh, depending on the given problem. The PDE's for these two modules are  
 195 solved based on their corresponding mesh, but can communicate a common parameter  
 196 to each other. In this model, the common parameters (the stresses) are calculated in  
 197 the description of the contact mechanics through an external MATLAB<sup>®</sup> script and are  
 198 fed into both COMSOL<sup>®</sup> modules, adapted to the appropriate mesh of the module.  
 199 To qualitatively illustrate the simulation procedure and results, a model consisting of  
 200 a rectangular block of aluminum of dimension 18 cm-by-10 cm-by-1 cm in  $x$ ,  $y$  and  $z$   
 201 direction will be considered. On the largest surface of the block, at  $z = 0$  m and centered  
 202 about  $x = 0.05$  m and  $y = 0.05$  m, a circular zone with a diameter of 1 cm acts as a  
 203 transducer, exerting a normal displacement in the form of a continuous sinusoidal wave  
 204 of frequency 70 kHz, with an amplitude of 100 nm. Two different defects are studied.  
 205 A first synthetic 2D defect in the form of a zero thickness cut is considered located at  
 206  $x = 15$  cm. The cut is oriented perpendicular to the surface, 3.3 cm deep and runs  
 207 through the full 1 cm depth of the sample. A second zero thickness defect has a more  
 208 complex shape, where the defect is open at the front and top side of the sample, while  
 209 the geometry of the defect is closed through the material. The defect is curved in all  
 210 three dimensions, runs to the same depth of 3.3 cm depth and the opening at the front  
 211 side is located at the same place of the first defect. A normal prestress is applied at the  
 212 defect interface for both studied defects, to increase the time spent in contact, allowing  
 213 for a larger amount of time where the defect experiences friction instead of clapping.  
 214 The geometry of both these defects are taken as such to test either a planar cut through  
 215 the whole sample and a more complex defect which does not run through the whole  
 216 sample and is curved. The areas around both defects is meshed denser than the other  
 217 region of the sample. The meshdensity in the healthy region of the sample is meshed  
 218 at 12 elements for each wavelength, whereas the denser region consists of 84 elements  
 219 for each wavelength. Not only is this area denser to propagate the higher harmonics  
 220 generated by the clapping and friction of the defect, it is also needed to obtain a stable  
 221 contact description. All mesh elements are quadratic.

### 222 3. Results

223 First, the planar defect will be discussed, after which the more complex geometry is  
 224 treated. These two different defects are studied in order to have a benchmark for the  
 225 model (planar defect), which is used to study the numerical stability and performance  
 226 of the model. The second defect is introduced in order to observe the results of a more  
 227 realistic defect.

#### 228 3.1. Planar defect

229 Figure 4 displays the frequency spectrum of the normal displacement,  $u_z$ , at a  
 230 point on the  $x$ - $y$  plane near the planar defect region. It can be clearly seen that higher

231 harmonics of the excitation frequency are present in the response signal. To ensure that  
 232 these harmonics directly originate from the defect, the amplitudes at the fundamental  
 233 frequency and its higher harmonics were examined on the surface of the sample and their  
 234 distribution is visualized in Figure 5 for the displacement tangential to the defect and in  
 235 Figure 6 for the displacement in the normal direction to the defect. The results reveal a  
 236 concentration of the magnitudes of the second and third harmonic in the neighbourhood  
 237 of the defect and confirm that the origin of these generated frequencies is to be attributed  
 238 to the interaction of its interfaces: friction (Figure 5) and clapping (Figure 6). From  
 239 Figures 5 and 6a, b and c it can be concluded that the harmonics are predominantly  
 240 generated near the tip of the defect, the reason being that the region of the crack tip  
 241 experiences more stress, compared to the open end of the crack. This is in agreement  
 242 with experimental observations reported in previous research studies [17].

243 Apart from the acoustic spectrum, the multiphysics model also allows to produce a  
 244 map of the thermal response as an output to study. It is expected that the temperature  
 245 increases as a result of energy dissipated from friction at the defect's interface. Figure 7  
 246 displays the temperature increase on the planar surface of the defect (i.e. the partial part  
 247 of the  $y$ - $z$  plane at  $x = 0.15$  m, covering only the defected area and no healthy material).  
 248 Again, the crack tip reveals the highest temperature increases. In addition, some smaller

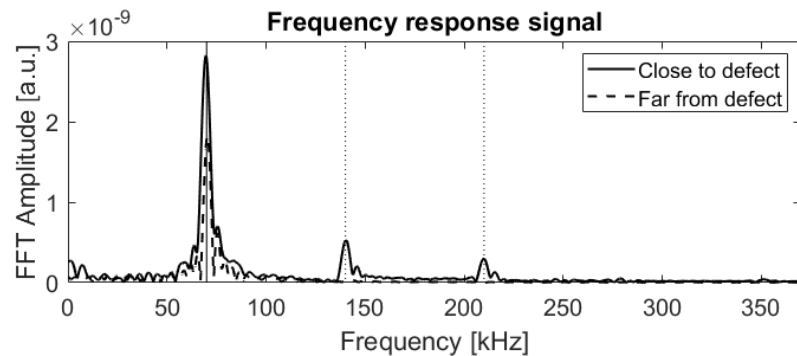


**Figure 4.** Generation of higher harmonics of the applied frequency, as a result of the friction and clapping of the interfaces of a zero-thickness, planar cut.

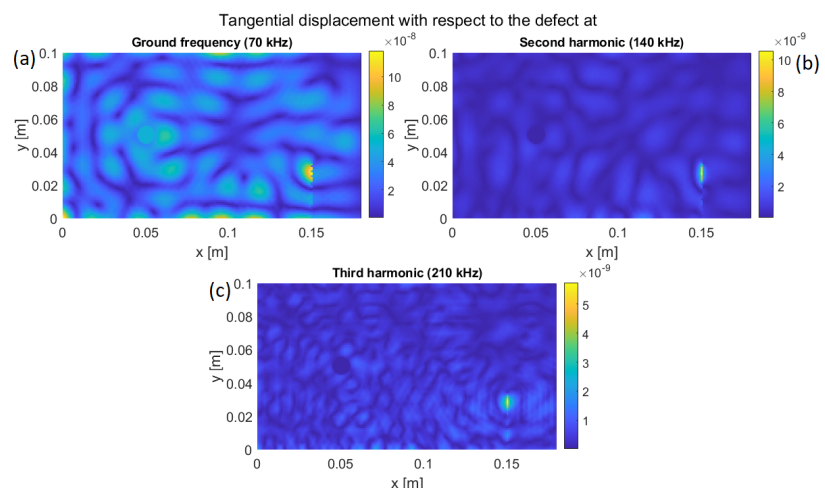


**Figure 5.** Source of the harmonics of the excitation frequency in a rectangular aluminum block containing a vertical cut at  $x = 0.15$  m extending between  $y = 0$  m and  $y = 0.033$  m. Figure 4a displays the amplitude of the tangential displacement, with relation to the defect, at each location on the surface ( $z = 0$  m), calculated by selecting the Fourier transform magnitude at the excitation frequency. Figures 4b and 4c shows the magnitudes of the same signals for the second and the third harmonic respectively.



249 temperature effect is present near the open edge of the crack. Within the small total  
 250 simulation time, the temperature distribution is only affected close to the defect's region,  
 251 as the timescale of the overall thermal response is much larger compared to the acoustic  
 252 timescale and the timescale of the contact physics. To illustrate this, Figure 8 shows the  
 253 region of the front surface ( $z = 0$  m near the defect, revealing only a thin dissipation  
 254 zone of the generated heat through the sample. Following Equation 4, temperature  
 255 increases can be achieved as a result of either a relative large displacement or/and a  
 256 large stress. The region near the crack tip experiences a large amount of friction, as the  
 257 higher harmonics are originating from that location, and therefore also temperature will  
 258 increase from this local heat source. At the crack tip itself however, the asperities of  
 259 the rough surfaces will be locked, making it unable to displace them and to experience  
 260 rubbing. Therefore, heating as a result of friction does not take place at the very tip of  
 261 the defect itself, but only near that area. In addition, the part of the defect that opens  
 262 up near the free side of the sample also appears to engender an increase of the local  
 263 temperature and of its surrounding. The component from Equation 4 responsible for this  
 264 is the relative tangential displacement, as this part of the defect can move more freely.

### 265 3.2. Defect with a complex geometry

266 Again, the amplitudes at the fundamental frequency and its higher harmonics were  
 267 examined on the surface of the sample and their distribution is visualized in Figure 9 for  
 268 the displacement tangential to the defect and in Figure 10 for the displacement in the  
 269 normal direction to the defect. The results reveal a concentration of the magnitudes of  
 270 the second and third harmonic in the neighbourhood of the defect and confirm that the  
 271 origin of these generated frequencies is to be attributed to the interaction of its interfaces:  
 272 friction (Figure 9) and clapping (Figure 10). Friction is more present at the closed part  
 273 of the defect, whereas clapping is more present at the open part, as is retrieved from  
 274 both figures. From Figures 9 and 10a, b and c it can be concluded that the harmonics are  
 275 generated along the length of the defect, the reason being that the region of the crack  
 276 tip experiences more stress, compared to the open end of the crack, but the open end  
 277 experiences more movement compared to the closed part. This is in agreement with  
 278 experimental observations reported in previous research studies [17].

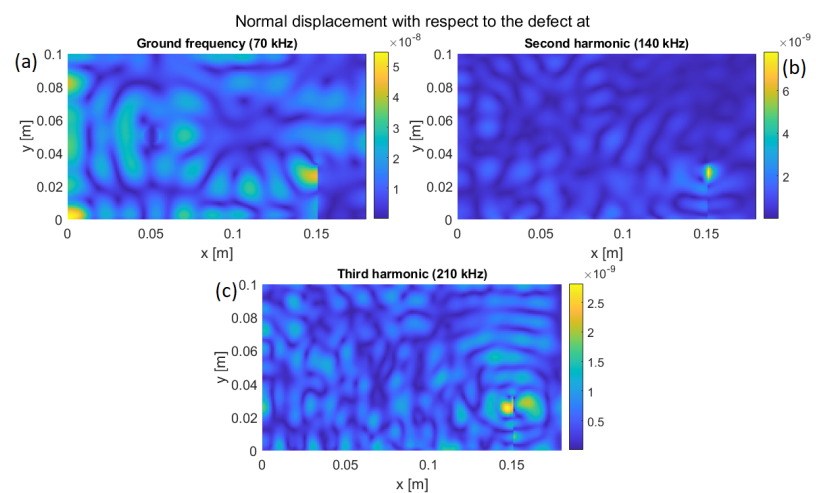


**Figure 6.** Source of the harmonics of the excitation frequency in a rectangular aluminum block containing a vertical cut at  $x = 0.15$  m extending between  $y = 0$  m and  $y = 0.033$  m. Figure 5a displays the amplitude of the normal displacement, with relation to the defect, at each location on the surface ( $z = 0$  m), calculated by selecting the Fourier transform magnitude at the excitation frequency. Figures 5b and 5c shows the magnitudes of the same signals for the second and the third harmonic respectively.

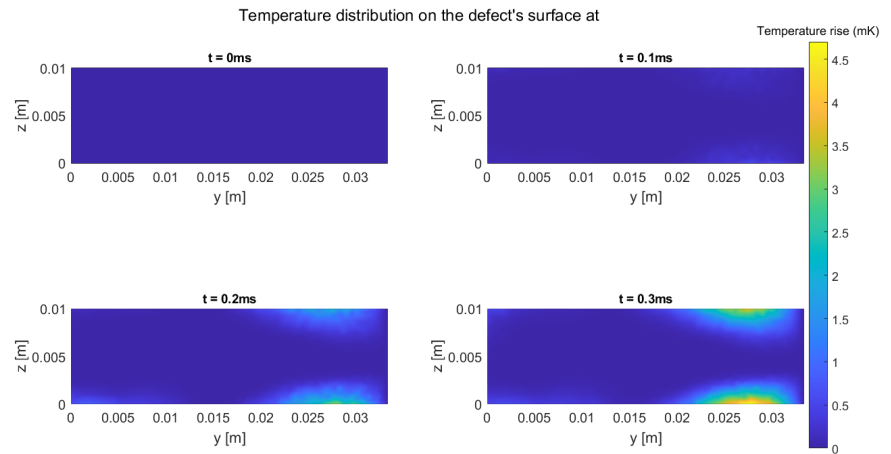


**Figure 7.** Temperature increase at the defect's surface (partial  $y$ - $z$  plane at  $x = 0.15$  m over 4 time instances, covering the full defected area without any undamaged part of the sample. The highest temperature increase occurs at surfaces  $z = 0$  m and  $z = 0.1$  m near the crack tip ( $y = 0.033$  m) with some smaller temperature increase also being present at the open edge of the crack.

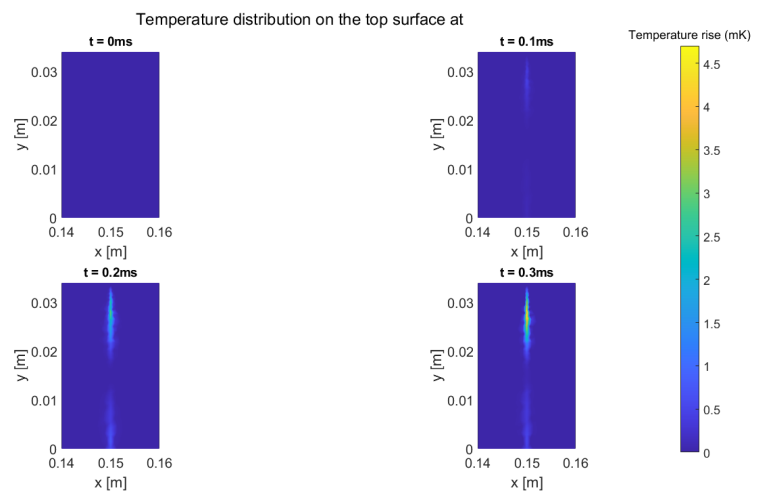


**Figure 8.** Thermal view from the surface ( $z = 0$ ) of the specimen zoomed in on the region of the defect, showing that the increase in temperature is highest at the edges (tip and open end of the cut) and increases over time.

279 Apart from the acoustic spectrum, the multiphysics model also allows to produce a  
 280 map of the thermal response as an output to study. It is expected that the temperature  
 281 increases as a result of energy dissipated from friction at the defect's interface. Within  
 282 the small total simulation time, the temperature distribution is only affected close to the  
 283 defect's region, as the timescale of the overall thermal response is much larger compared  
 284 to the acoustic timescale and the timescale of the contact physics. To illustrate this,  
 285 Figure 11 shows the region of the front surface ( $z = 0$  m near the defect, revealing only a  
 286 thin dissipation zone of the generated heat through the sample. Following Equation 4,  
 287 temperature increases can be achieved as a result of either a relative large displacement

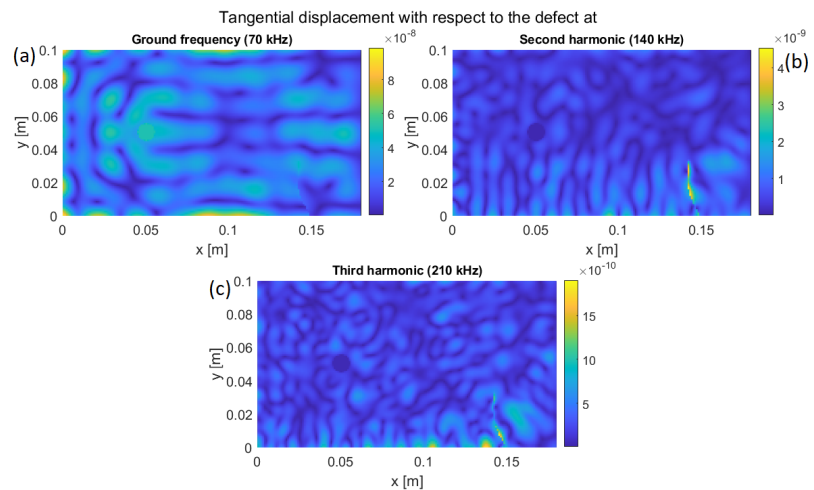


**Figure 9.** Source of the harmonics of the excitation frequency in a rectangular aluminum block containing a vertical cut at  $x = 0.15$  m extending between  $y = 0$  m and  $y = 0.033$  m. Figure 8a displays the amplitude of the tangential displacement, with relation to the defect, at each location on the surface ( $z = 0$  m), calculated by selecting the Fourier transform magnitude at the excitation frequency. Figures 8b and 8c shows the magnitudes of the same signals for the second and the third harmonic respectively.

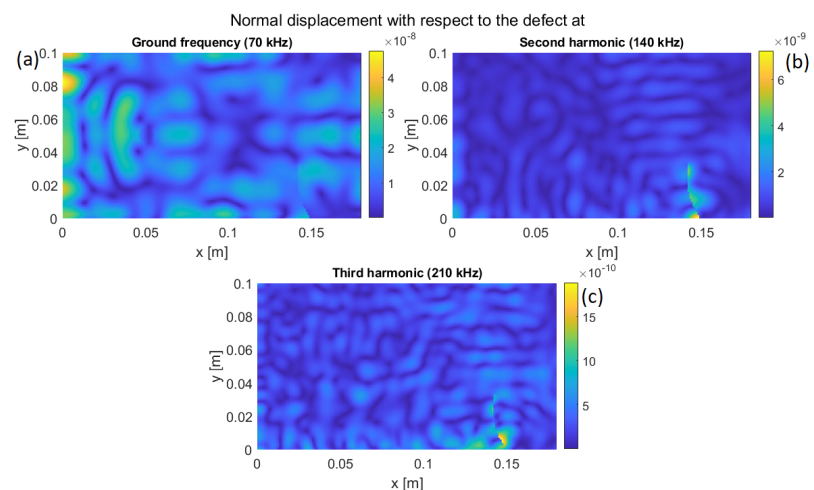


**Figure 10.** Source of the harmonics of the excitation frequency in a rectangular aluminum block containing a vertical cut at  $x = 0.15$  m extending between  $y = 0$  m and  $y = 0.033$  m. Figure 9a displays the amplitude of the normal displacement, with relation to the defect, at each location on the surface ( $z = 0$  m), calculated by selecting the Fourier transform magnitude at the excitation frequency. Figures 9b and 9c shows the magnitudes of the same signals for the second and the third harmonic respectively.

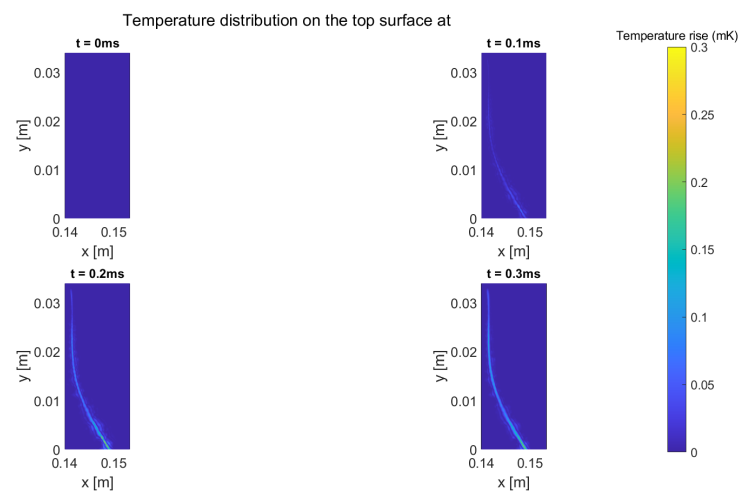


**Figure 11.** Thermal view from the surface ( $z = 0$ ) of the specimen zoomed in on the region of the defect, showing that the increase in temperature is highest at the edges (tip and open end of the cut) and increases over time.

288 or/and a large stress. In addition, the part of the defect that opens up near the free  
 289 side of the sample also appears to engender an increase of the local temperature and  
 290 of its surrounding. The component from Equation 4 responsible for this is the relative  
 291 tangential displacement, as this part of the defect can move more freely.

#### 292 4. Discussion and conclusion

293 The results of the above qualitative study confirm that the presence of higher  
 294 harmonics of the excitation frequency is related to the nonlinear behaviour of the defect  
 295 when it experiences friction and clapping as a result from an acoustic excitation [18–  
 296 20]. The appearance of a rather large defect (3.3 cm-by-1 cm) can be revealed through  
 297 the mapping of these nonlinearities in the acoustic spectrum, as these harmonics are  
 298 originating from the defect, cfr. Figure 5, 6, 9 and 10 [17,21,22]. In addition, the zone of  
 299 the surface breaking crack that activates these higher harmonics is similar to literature  
 300 reportings. For instance, Fierro et al. performed experiments on a fatigue surface  
 301 breaking crack in an aluminium plate and demonstrated that the zones that generated  
 302 the second harmonic were located near the crack tip [23].

303 With respect to the thermal response of a dynamical action, Renshaw et al. reported  
 304 that heating due to dissipation of energy when surfaces experience friction is one of  
 305 the most significant heating mechanisms during vibrothermography [24]. Rizi et al.  
 306 developed a phenomenological 3D model to describe the energy dissipated by friction  
 307 [25]. In both works, the authors communicated that the temperature primarily increases  
 308 in a region close to the crack tip, where the asperities are not locked, far more than  
 309 compared to the crack region near the open part of the specimen or the crack tip itself.  
 310 These findings were also confirmed in the above mentioned study of Fierro et al. [23].

311 Analyzing the results obtained with our computational model, it can this be con-  
 312 cluded that qualitatively, the presently developped 3D model successfully accounts for  
 313 the generation of higher harmonics and the origin of heat within both a planar defect and  
 314 a more complex defect at locations that are in agreement with pioneering reports found  
 315 in literature, handling both 2D computational models and experiments. Even though the  
 316 input parameters of the model were not specifically tuned to match a real experiment,  
 317 the actual temperature increases lay within the expected range. More quantitative results  
 318 can be obtained on a case by case basis. Currently, the main drawback of the simulation  
 319 tool is that the three dimensional computational model requires a lot of computational  
 320 time. For instance, for the specific model discussed here, it took three days to run the  
 321 0.3 ms simulation on a desktop.

322 In the future, we will address more quantitative studies of the developed model,  
323 including anisotropic materials, and investigate adaptations to reduce the computational  
324 time of the model to acceptable execution times.

325 **Author Contributions:** Conceptualization, K.T., V.A. and K.VDA; methodology, K.T. and V.A.;  
326 software, K.T.; validation, K.T.; formal analysis, K.T.; investigation, K.T.; resources, K.T. and K.VDA;  
327 data curation, K.T.; writing—original draft preparation, K.T.; writing—review and editing, K.VDA.;  
328 visualization, K.T.; supervision, K.VDA.; project administration, K.VDA.; funding acquisition,  
329 K.VDA and V.A. All authors have read and agreed to the published version of the manuscript.

330 **Funding:** The research leading to these results has gratefully received funding from Internal  
331 Funds KU Leuven (C24/15/021) and joint doctorate financing by I-SITE ULNE and KU Leuven.  
332 One of authors (Vladislav Aleshin) is also grateful to the Tomsk State University competitiveness  
333 improvement program.

334 **Conflicts of Interest:** The authors declare no conflict of interest.

## References

1. Delrue, S.; Van Den Abeele, K. Three-dimensional finite element simulation of closed delaminations in composite materials. *Ultrasonics* **2012**, *52* 315–324
2. Blanloeuil, P.; Meziane, A.; Bacon, C. Numerical study of nonlinear interaction between a crack and elastic waves under an oblique incidence. *Wave Motion* **2014**, *51* 425–437
3. Plum, R.; Ummenhofer, T. Structural-thermal finite element simulation of vibrothermography applied to cracked steel plates. *Quant. Infrared Thermogr. J.* **2011**, *8* 201–220
4. Aleshin, V.V.; Delrue, S.; Trifonov, A.; Bou Matar, O.; Van Den Abeele, K. Two dimensional modeling of elastic wave propagation in solids containing cracks with rough surfaces and friction - Part I: Theoretical background. *Ultrasonics* **2018**, *82* 11–18.
5. Delrue, S.; Aleshin, V.V.; Truyaert, K.; Bou Matar, O.; Van Den Abeele, K. Two dimensional modeling of elastic wave propagation in solids containing cracks with rough surfaces and friction – Part II: Numerical implementation. *Ultrasonics* **2018**, *82* 19–30.
6. Wang, D.; De Boer, G.; Neville, A.; Ghanbarzadeh, A. A new numerical model for investigating the effect of surface roughness on the stick and slip of contacting surfaces with identical materials. *Tribology International* **2021**, *159* 106947
7. Bonari, J.; Paggi, M.; Reinoso, J. A framework for the analysis of fully coupled normal and tangential contact problems with complex interfaces. *Finite Elements in Analysis and Design* **2021**, *196* 103605
8. Truyaert, K.; Aleshin, V.V.; Delrue, S.; Van Den Abeele, K. A Multiscale Numerical Model for Structures with Internal Frictional Contacts. In *Proceedings of the 1st International Conference on Numerical Modelling in Engineering Volume 2: Numerical Modelling in Mechanical and Materials Engineering*. Springer, Singapore, 2019, pp. 77–89.
9. Truyaert, K.; Aleshin, V.; Van Den Abeele, K.; Delrue, S. Theoretical calculation of the instantaneous friction-induced energy losses in arbitrarily excited axisymmetric mechanical contact systems. *Int. J. Solids Struct.* **2019**, *158*, 268–276.
10. Barber, J.; Davies, M.; Hills, D. Frictional elastic contact with periodic loading. *Int. J. Solids Struct.* **2011**, *48* 2041–2047
11. Putignano, C.; Ciavarella, M.; Barber, J. Frictional energy dissipation in contact of nominally flat rough surfaces under harmonically varying loads. *J. Mech. Phys. Solids* **2011**, *59* 2442–2454
12. Mindlin, R.; Deresiewicz, H. Elastic spheres in contact under varying oblique forces. *J. Appl. Mech.* **1953**, *20* 327–344
13. Jäger, J. Axi-symmetric bodies of equal material in contact under torsion or shift. *Archive of Applied Mechanics* **1995**, *65*(7) 478–487
14. Ciavarella, M. The generalized Cattaneo partial slip plane contact problem. I—Theory. *International Journal of Solids and Structures* **1998**, *35*(18) 2349–2362
15. Biwa, S.; Nakajima, S.; Ohno, N. On the acoustic nonlinearity of solid-solid contact with pressure-dependent interface stiffness. *J. Appl. Mech.*, **2004**, *71.4* 508–515
16. Yuan, M.; Lee, T.; Kang, T.; Zhang, J.; Song, S. J.; Kim, H. J. Absolute measurement of ultrasonic non-linearity parameter at contact interface. *Nondestructive Testing and Evaluation* **2015**, *30*(4) 356–372
17. Ulrich, T. J.; Sutin, A.M.; Guyer, R.A.; Johnson, P.A. Time reversal and non-linear elastic wave spectroscopy (TR NEWS) techniques. *International Journal of Non-linear Mechanics* **2008**, *43* 209–216
18. Van Den Abeele, K. A.; Johnson, P. A.; Sutin, A. Nonlinear elastic wave spectroscopy (NEWS) techniques to discern material damage, part I: nonlinear wave modulation spectroscopy (NWMS). *Journal of Research in Nondestructive Evaluation* **2000**, *12*(1) 17–30.
19. Yuan, M.; Zhang, J.; Song, S. J.; Kim, H. J. Numerical simulation of Rayleigh wave interaction with surface closed cracks under external pressure. *Wave Motion* **2015**, *57* 143–153.
20. Delrue, S.; Tabatabaeipour, M.; Hettler, J.; Van Den Abeele, K. Applying a nonlinear, pitch-catch, ultrasonic technique for the detection of kissing bonds in friction stir welds. *Ultrasonics* **2016**, *68* 71–79.
21. Solodov, I.; Rahammer, M.; Derusova, D.; Busse, G. Highly-efficient and noncontact vibro-thermography via local defect resonance. *Quantitative InfraRed Thermography Journal* **2015**, *12*(1) 98–111.

22. Solodov, I.; Bai, J.; Bekgulyan, S.; Busse, G. A local defect resonance to enhance acoustic wave-defect interaction in ultrasonic nondestructive evaluation. *Applied Physics Letters* **2011**, *99*(21) 211911.
23. Fierro, G. P. M.; Ginzburg, D.; Ciampa, F.; Meo, M. Nonlinear ultrasonic stimulated thermography for damage assessment in isotropic fatigued structures. *Journal of Sound and Vibration* **2017**, *404* 102–115.
24. Renshaw, J.; Chen, J. C.; Holland, S. D.; Thompson, R. B. The sources of heat generation in vibrothermography. *NDT& E International*, **2011**, *44*(8) 736–739.
25. Rizi, A. S.; Hedayatrasa, S.; Maldague, X.; Vukhanh, T. FEM modeling of ultrasonic vibrothermography of a damaged plate and qualitative study of heating mechanisms. *Infrared Physics & Technology* **2013**, *61* 101–110.